Statistical Study of Rainfall Inversion Using the Earth-Space Link at the Ku Band: Optimization and Validation for 1 Year of Data

Yingcheng Zhao, Xichuan Liu, Minghao Xian, and Taichang Gao

***Abstract*—The large-scale monitoring of rainfall is of great significance in the research of meteorology, hydrology, and atmospheric measurement science. In recent years, with the quick development of communication satellite constellation, the use of earth-space link (ESL) to measure rainfall in the atmosphere is expected to be a potential approach for the large-scale monitoring of global rainfall. In this article, to verify the long-term performance of rainfall measurement using ESL, the data of an ESL at the Ku band and a Thies Laser Precipitation Monitor (LPM) in Nanjing were collected. The rainfall inversion model using ESL was optimized according to the height of 0 °C-layer from the radiosonde data of ten years, and the inversion results in the different types of rainfall were discussed. The results show that the rainfall inversed by the optimized ESL model are in good agreement with the rainfall measured by LPM (correlative coefficient is 0.985), the relative errors of rain intensity inversed by ESL in light rain, moderate rain, heavy rain, and extreme rain are 20%, 15.17%, 8.93%, and 8.99%, respectively. The average relative errors of rain intensity measured by the ESL in convective rainfall and stratiform rainfall are 16.01% and 26.59%, respectively.**

***Index Terms*—Earth-space link (ESL), long-term performance, rainfall attenuation, rainfall inversion, statistical analysis.**

I. Introduction

As a common weather phenomenon in the troposphere, rainfall affects all the aspects of the human and society. The instability of rainfall in time and nonuniformity in space will bring about natural disasters such as landslides, floods, and droughts [1]. Therefore, the real-time monitoring of rainfall with high precision and high temporal and spatial resolution is of great significance in the meteorological and hydrological science and application [2]. At present, the operational methods for the measurement and inversion of near-surface rainfall are rain gauges, weather radars, and meteorological satellites [3]. Rain gauges can accurately measure rainfall on the ground, and weather radars and meteorological satellites can provide a wide range of spatial distributions of precipitation [4], [5]. Through the data fusion of rain gauges, weather radars, and meteorological satellites, it is expected to obtain the precipitation field with higher precision and temporal and spatial resolution. However, limited by the high cost and complex maintenance requirements, rain gauges and weather radars are unevenly distributed all over the world.

With the development and application of radio communication technology in the world [6], a new rainfall measurement method using the attenuation of microwave links has emerged in the recent years [7], [8]. Besides the horizontal microwave links (HMLs) [9]–[11] between the ground base stations, the microwave link between a satellite and the ground receiving station above the earth will also receive data on the absorption and scattering of rainfall propagating in the atmosphere, thus resulting in the attenuation of signal energy [12]. As a result, the oblique microwave links [also called earth-space link (ESL)] between the satellite and the ground station are also applied to measure the rainfall [13], [14].

Differently from HMLs, the ESL has the lowest technical requirements and can be easily installed in any location, since the ESL consists of a receiver and a common paraboloid antenna for television [15]. And this method has attracted wide attention from scholars in many countries because of its low cost and high resolution. Barthès *et al.* [13] carried out experiments in Paris and found that the discrepancies between radar observations and ESL could be as high as 30% in the case of 1-h accumulated rainfall. In order to test the performance of ESL in retrieving rainfall, Arslan *et al.* [16] used the satellite signal attenuation at Ku band to the estimated path-integrated rain rate along the link path, and compared the results with rainfall accumulations obtained using weather radar measurements along the same path. The results showed that the retrieval performance of ESL to light rain below 1.5 mm/h was not good [17]. Except for a single link, Huang *et al.* [18], [19] demonstrated the feasibility of using an ESL network to detect spatial rainfall fields through simulation experiments [20]. And the NEFOCAST research project, funded by the government of the Tuscany region (Italy), made opportunistic use of broadcast satellite signals related to domestic services to estimate the rain intensity [21], [22]. In addition, Xian *et al.* [23] improved the model of rainfall inversion by ESL based on the melting layer, and proposed a method for the reconstruction of horizontal and vertical rainfall fields [24].

The previous studies have focused on case study or short-term rainfall events, the long-term performance of rainfall inversion

Manuscript received June 28, 2021; revised August 16, 2021; accepted September 6, 2021. Date of publication September 9, 2021; date of current version September 30, 2021. This work was supported in part by the National Natural Science Foundation of China under Grant 41975030, Grant 41505135, and Grant 41475020. *(Corresponding author: Xichuan Liu.)*

The authors are with the College of Meteorology and Oceanography, National University of Defense Technology, Changsha 410003, China (e-mail: zhaoyingcheng17@foxmail.com; liuxc2012@hotmail.com; xmh1995@foxmail.com; 2009gaotc@gmail.com).

Digital Object Identifier 10.1109/JSTARS.2021.3111336

TABLE I
PARAMETERS OF ESL

Antenna coordinates	31°58′27″N, 118°48′52″E
Antenna altitude	29 m
Satellite altitude	35786 km
Frequency	12.32 GHz (Ku band)
Polarization mode	Vertical polarization
Elevation angle	47.87°

using ESL still need to be evaluated. In this article, we optimize the rainfall inversion model in the selection of 0 °C-layer by ESL and test the model using the measured data of ESL for a whole year. The inversed rainfall and the accuracy of rainfall in the different categories of rain intensity are compared with the data of Thies Laser Precipitation Monitor (LPM) in the same location. Furthermore, different types of rainfall are analyzed. The results are expected to provide fundamentals for the practical application of rainfall measurement using ESL in the near future.

The rest of this article is organized as follows. Section II describes the experimental setting and data selection, and introduces the principle of measuring rainfall by ESL in detail. Section III provides a comparative analysis and discussion of the results, and analyzes the performance of ESL inversions of different types of rainfall. Finally, Section IV concludes the article.

II. MATERIAL AND METHODS

A. Experimental Setup and Data

To verify the feasibility and evaluate the performance of rainfall inversion by using the attenuation of ESL, a set of ESL device at the Ku band was built in Jiangning District, Nanjing, China (31°58′27″ N, 118°48′52″ E) in July 2019. The specific parameters of ESL are shown in Table I. The device is mainly composed of a satellite antenna, ground receiver, and computer terminal. The satellite butterfly antenna has a diameter of 1.2 m, which is used to receive Ku-band signals (12.32 GHz) transmitted by the geostationary satellite AsiaSat5 located at 100.5 °E. The ground receiver converts the received signal through the low noise block converter and transmits it to the signal processing terminal. Finally, a corresponding signal-to-noise ratio (SNR) value is the output every 1 s. At the same time, we installed a Thies LPM beside the satellite antenna to measure rainfall synchronously. And the sounding data from Nanjing reference climate station can provide the 0 °C-layer height of local atmosphere, which is located at 9 km southeast of the satellite antenna. Fig. 1 shows the horizontal distribution of the experimental instruments in Nanjing.

We use the Ku-band ESL device built in Nanjing to carry out the field measurement of rainfall and obtain statistics on the annual rainfall events from January to December 2020. The ground receiver in the device receives and processes one signal per second; therefore, the time resolution is 1 s. The original data received will oscillate periodically due to the orbit perturbation of the satellite, and we use the Kalman filter and difference algorithm to remove this periodic influence factor in the data quality control.

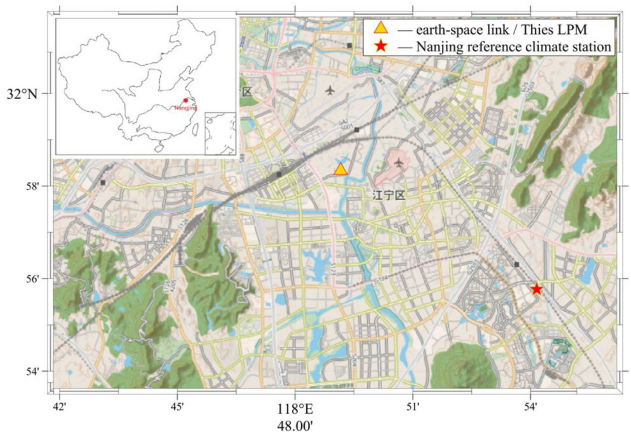

Fig. 1. Horizontal distribution of experimental equipment. The ESL is in the same position as the Thies LPM.

The Thies LPM installed in the same location as the ESL is a new generation of instruments made in Germany for precise detection of surface precipitation. This instrument has been installed in key areas of many countries for automatic observation of precipitation. It uses a 780 nm laser beam which is 228 mm long, 20 mm wide, and 0.75 mm thick on average, resulting in a sampling area of 45.6 cm^2. The measured values of the size and velocity are processed by a digital signal processor, and checked for plausibility. The measuring range of droplet diameter is between 0.16 and 8 mm, the measuring range of particle velocity is between 0.2 and 20 m/s, and the measuring range of rain intensity is between 0.005 and 250 mm/h (light rain to extreme rain). Thies LPM shows the characteristics of high resolution and accuracy, and it is well suited for the measurement and detection of different types of precipitation such as drizzle, rain, hail, snow, and mixed precipitation [25], [26]. In this article, the rainfall estimated by ESL is compared with the measured value of Thies LPM, and the performance of ESL is analyzed.

While the ESL measures rainfall, the annual rainfall measured by Thies LPM installed can be used as a reference value for the measurement results of the ESL. Since Thies LPM outputs one rain intensity every 1 min, to ensure that the measurement results of the ESL are comparable to those of the Thies LPM, the time resolution of the ESL needs to be averaged from 1 s to 1 min.

B. Description of the Measurement Principle

The basic principle of rainfall inversion using ESL is described as follows. When rainfall occurs in the path between the satellite and the antenna, the microwave signal transmitted by the satellite will be weakened. The total attenuation of microwave signal transmission can be obtained through the real-time recordings of the ground receiver. Then, the microwave rain attenuation can be obtained by using the corresponding microwave rain attenuation extraction algorithm. At this time, the average rain intensity on the transmission path of the ESL can be obtained by using the relationship between microwave rain attenuation and rainfall [27], [28].

The microwave signal of the ESL will attenuate due to the absorption and scattering of raindrops. The total attenuation on the whole link can be regarded as the accumulation of the attenuation effect of all raindrops that appear on the path of the link. According to the research of Xian *et al*. [28], the attenuation coefficient γ_R (dB/km) of rainfall on the ESL can be expressed as

$$\gamma_R = 10\log e \int_0^\infty \frac{\pi D^2}{4} C_{\text{ext}}(D) N(D) dD \tag{1}$$

where D is the equivalent diameter used to characterize the raindrop size, $C_{\text{ext}}(D)$ is the extinction cross section of the particles that can be calculated using the T-matrix algorithm, and $N(D)$ represents the raindrop size distribution (DSD) along the link. After years of research on ESL, a number of widely used attenuation models have been proposed. These models include the Crane model [29], SAM simple attenuation model [30], and ITU-R model [31]. Among them, the γ–R relation of the ITU-R model is the most widely used. In this model, the relationship between the average rain intensity R (mm/h) and the rainfall attenuation coefficient γ_R on the ESL is

$$\gamma_R = \alpha R^\beta. \tag{2}$$

The values of the coefficients α and β in the above formula are related to the frequency of the radio signal, the polarization mode, the polarization inclination angle relative to the horizontal position, and the DSD [32]. If the length of the ESL in the rainfall area is L_R (km) and the rainfall is evenly distributed on the path, then the attenuation caused by rainfall A_R (dB) can be written as

$$A_R = \alpha R^\beta L_R. \tag{3}$$

In the calculation of the actual ESL to measure rainfall, L_R can be expressed as the 0 °C-layer height h_0 (km) of the atmospheric as follows[28], [33]:

$$L_R = (h_0 + 0.36)/\sin\theta \tag{4}$$

where θ is the elevation of the ESL. In this way, the average rain intensity R of the link can be obtained as follows:

$$R = \left[A_R \sin\theta/(h_0 + 0.36)\,\alpha\right]^{\beta^{-1}}. \tag{5}$$

For the Ku band, the values of α and β can be determined in ITU-R recommendation P.838-3 [32]. Therefore, in the calculation for retrieving rainfall using the ESL, when the attenuation A_R caused by rainfall is known, the average rain intensity R on the path can be obtained.

C. Signal Attenuation Model

When rainfall occurs in the atmosphere, the microwave signals transmitted by the satellites reach the satellite antenna on the ground through the ESL and are transmitted to the receiver for signal processing. When we express the transmitting power of the satellite with P_t, the receiving power P_r of the ground receiver can be expressed as [24]

$$\mathrm{P}_r(t) = P_t(t) \cdot G \cdot \eta_A \cdot \eta_F \cdot \eta_R + P_n(t) \tag{6}$$

where G is the antenna gain, P_n is the noise power of the signal, and η_A represents the attenuation coefficient of nonrainy factors in the atmosphere; such as the gas composition and cloud and atmospheric turbulence. In addition, η_F and η_R represent the attenuation coefficients of microwaves in free space and rainfall regions, respectively. Therefore, as far as the SNR of the receiver is concerned, the expression in decibels can be given as

$$SNR(t) = 10\log\frac{P_t(t) \cdot G \cdot \eta_A \cdot \eta_F \cdot \eta_R}{P_n(t)}. \tag{7}$$

The path-integrated rainfall attenuation A_R of the microwave in the rainfall area can be described as

$$A_R(t) = -10\log(\eta_R) \tag{8}$$

and the attenuation A_F of microwaves in free space is written as

$$A_F(t) = -10\log(\eta_F). \tag{9}$$

Then (7), which describes the SNR of the receiver, can be written as

$$\mathrm{SNR}(t) = 10\log\frac{P_t(t) \cdot G \cdot \eta_A}{P_n(t)} - A_R(t) - A_F(t). \tag{10}$$

Noise power P_n mainly comes from system noise and sky noise, which can be given by

$$P_n(t) = k_B \cdot B \cdot (T_{\text{sys}}(t) + T_{\text{sky}}(t)) \tag{11}$$

where k_B represents the Boltzmann constant, B is the bandwidth of the satellite signal, and T_{sys} and T_{sky} represent the temperature of the signal receiving system and the sky, respectively. When rainfall occurs, T_{sys} can be assumed to be a fixed constant. At this time, the sky noise received by the receiver mainly comes from rainfall and is a function of rainfall attenuation A_R. For a fixed solid angle Ω, when considering the influence of the antenna beam pattern, T_{sky} is usually expressed as [34]

$$T_{\text{sky}}(t) = \frac{\int G(t,\Omega) \cdot t_m (1-10)^{-\frac{A_R(t)}{10}} d\Omega}{\int G(t,\Omega)\, d\Omega} \tag{12}$$

where $G(t, \Omega)$ represents the antenna gain pattern when the solid angle Ω is fixed and t_m is the average temperature of the link path.

We simply deform (11) and rewrite it as

$$P_n(t) = k_B \cdot B \cdot T_{\text{sys}}(t) \cdot \frac{(T_{\text{sys}}(t) + T_{\text{sky}}(t))}{T_{\text{sys}}(t)} \tag{13}$$

and define

$$\begin{aligned} P_0(t) &= k_B \cdot B \cdot T_{\text{sys}}(t), \\ [2pt] F_n(t) &= 10\log\left(\frac{T_{\text{sys}}(t) + T_{\text{sky}}(t)}{T_{\text{sy_s}}(t)}\right), \\ [2pt] V(t) &= 10\log\frac{P_t(t) \cdot G \cdot \eta_A}{P_0(t)} \end{aligned} \tag{14}$$

and then (10) can be written as

$$\mathrm{SNR}(t) = V(t) - F_n(t) - A_R(t) - A_F(t). \tag{15}$$

When there is no rain in the atmosphere, the $\mathrm{SNR}_{\text{no-rain}}$ value received by the ESL can be used as the attenuation baseline

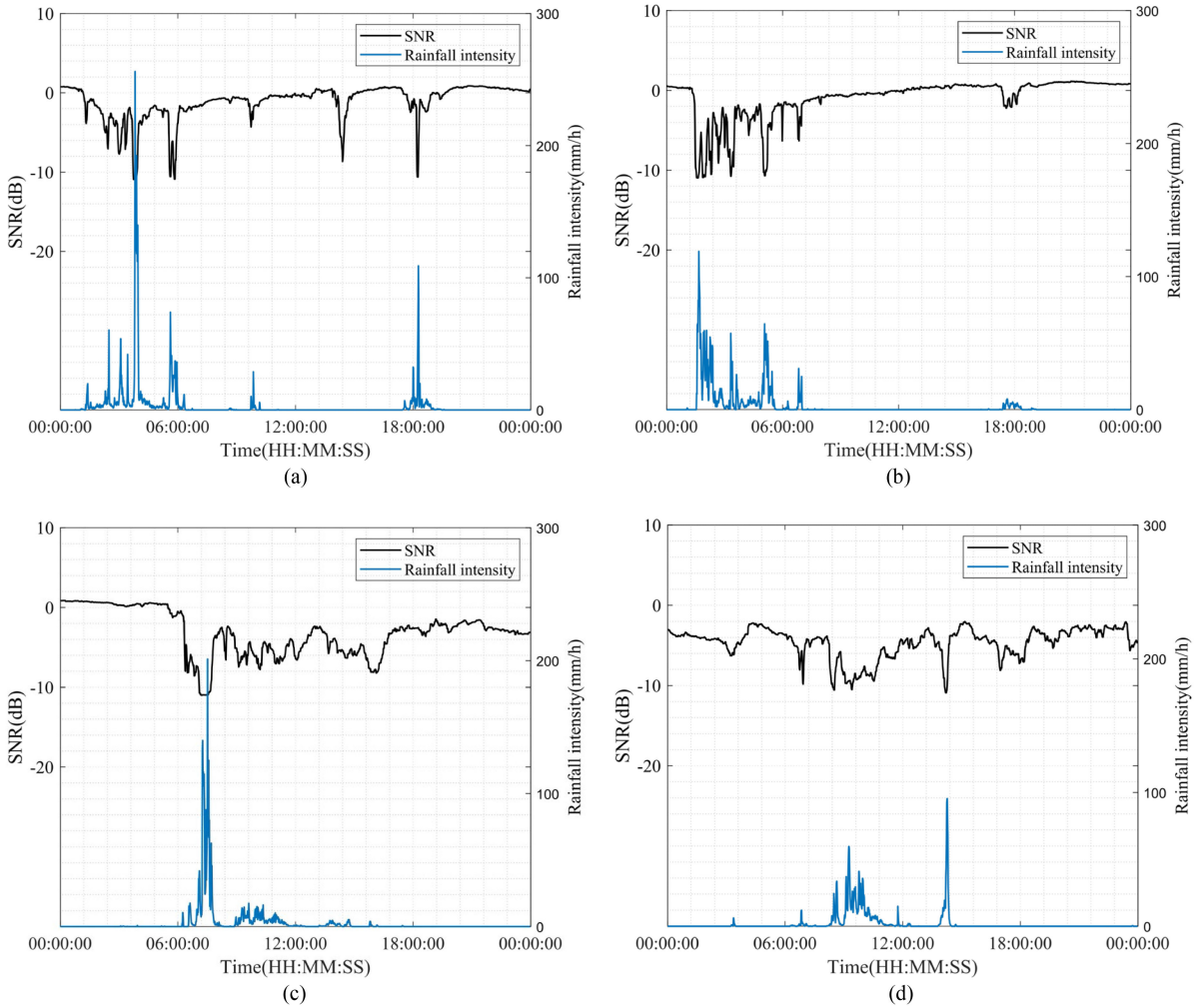

Fig. 2. Corresponding relationship between the rain intensity and the ESL signal for the rainfall event from June 13th to June 16th, 2020. The blue line is the rain intensity and the black line represents the SNR of the ESL.

$\mathrm{SNR}_{\mathrm{refer}}$; that is, the SNR of factors other than rainfall [24]

$$\mathrm{SNR}_{\mathrm{refer}} = \mathrm{SNR}_{\mathrm{no-rain}} = V(t) - F_n(t) - A_F(t). \quad (16)$$

Therefore, according to (15) and (16), the rainfall attenuation A_R can be written as

$$A_R(t) = \mathrm{SNR}_{\mathrm{refer}} - \mathrm{SNR}. \quad (17)$$

Finally, according to (5) and (17), we can write the average rain intensity retrieved from the ESL as

$$R = \left[\frac{(\mathrm{SNR}_{\mathrm{refer}} - \mathrm{SNR})\sin\theta}{(h_0 + 0.36)\,\alpha}\right]^{\beta^{-1}}. \quad (18)$$

To verify the correlation between the SNR of the microwave signal using the ESL and rainfall, we selected the significant continuous rainfall events from June 13th to June 16th in 2020 to analyze the relationship between the SNR of the signal and the rain intensity. As shown in Fig. 2, the SNR of the microwave signal of the ESL shows a rapid and irregular oscillation in a short period of time. This phenomenon is mainly caused by the movement of the atmosphere and the scintillation of the ionosphere. Although the SNR is affected by various factors in the atmosphere, rainfall is still the main meteorological factor for electromagnetic signals in the microwave band. When rainfall occurs in the atmosphere, the microwave signal of the ESL is weakened due to attenuation so that the SNR value of the signal is significantly reduced. There was no rain at the experimental site at approximately 14:00 on June 13th, but the SNR decreased. This may be related to the tilt of the ESL and the uneven spatial distribution of rainfall. Generally, the occurrence of rainfall can cause the SNR value to decrease obviously. Finally, through analysis and calculation, a negative correlation was observed between the SNR and the rain intensity, and the average correlation coefficient between them is approximately -0.721. The results show that the method of retrieving rainfall by using the SNR of the microwave signal of an ESL is feasible.

D. Optimization of the Model in the 0 °C-Layer Height

The 0 °C-layer height h_0 of the local atmosphere needs to be used when retrieving rainfall from the ESL. According to the relation formula (18) between the SNR and the rain intensity,

TABLE II
MONTHLY AVERAGE VALUE OF ATMOSPHERIC 0 °C-LAYER HEIGHT IN NANJING

Month	Jan	Feb	Mar	Apr	May	Jun	Jul	Aug	Sept	Oct	Nov	Dec
h_0(km)	1.06	1.37	2.24	3.38	4.29	4.85	5.28	5.28	4.85	3.93	2.82	1.46

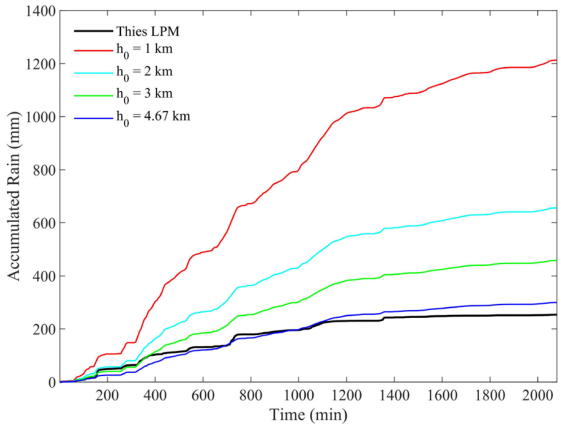

Fig. 3. For the rainfall events in July 2020, the accumulated rainfall measured by the ESL was compared with the measured value of the Thies LPM when different heights of the atmospheric 0 °C-layer was selected. The black line is the accumulated rainfall measured by the Thies LPM.

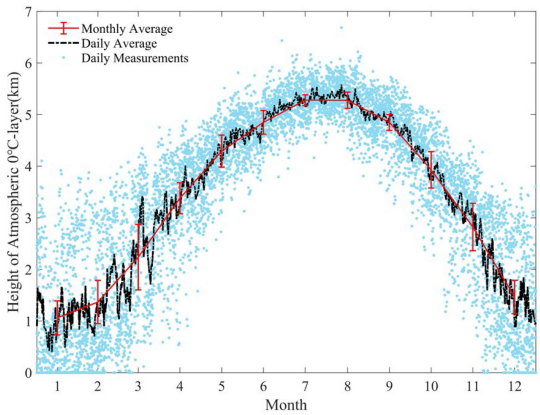

Fig. 4. Statistics of the height of the atmospheric 0 °C-layer in Nanjing in the last 10 years. The blue dots represent daily measurements, the black dotted line represents daily average, and the red solid line with error bars represents monthly average.

a higher height of h_0 corresponds to a smaller rain intensity, which is mainly because h_0 reflects the height of the rain layer to some extent. Under the same rainfall attenuation, a higher (lower) height of the top of the rain corresponds to a smaller (greater) rain intensity. In the previous studies, h_0 mostly uses statistical fixed constants. In ITU-R recommendation P.839 [24], the value of the atmospheric 0 °C-layer height h_0 in the Nanjing area can be taken as 4.67 km. As shown in Fig. 3, the accumulated rainfall recommended at 4.67 km in the ITU-R recommendation is indeed closer to the measured value of the Thies LPM than the other h_0 values.

To further study the characteristics of the actual atmospheric 0 °C-layer height, in this article, we use the radiosonde data of the Nanjing reference climate station over the last 10 years

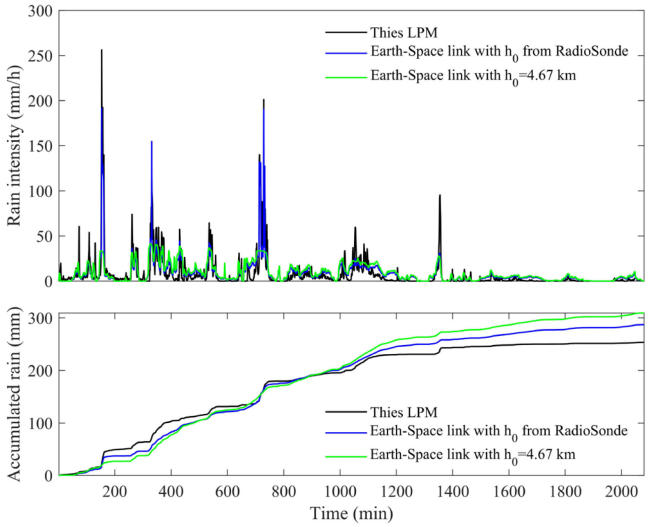

Fig. 5. For the rainfall events in July 2020, the rain intensity and accumulated rainfall measured by the ESL were compared with the measured values of the Thies LPM. The blue line and green line are the measurement results of the ESL when h_0 is based on the values obtained by radiosonde and the statistical values from the ITU-R recommendation, respectively. In addition, the black line is the measured value from the Thies LPM.

to study the variation characteristics of the local atmospheric 0 °C-layer. The statistical results of the atmospheric 0 °C-layer are shown in Fig. 4 and Table II. The analysis indicates that the local atmospheric 0 °C-layer height is not a fixed value throughout a year and has obvious seasonal variation characteristics [24]. Therefore, in the statistical analysis of the annual rainfall obtained using the ESL, the fixed statistical value of h_0 is not in line with the actual local situation. If h_0 adopts a fixed value, it will bring some measurement errors to the measurement results.

To solve this problem, to ensure that the value of the atmospheric 0 °C-layer height h_0 is consistent with the local actual situation and representative in rainfall received by the ESL, we apply the daily and monthly average values of h_0 obtained by radiosonde to the calculation model of the ESL to retrieve rainfall.

III. RESULTS AND DISCUSSION

A. Selection of 0 °C-Layer Height

In theory, the h_0 obtained by radiosonde can better represents the actual situation of the atmospheric 0 °C-layer height than the fixed statistical value given by ITU-R recommendation. To verify whether the atmospheric 0 °C-layer height h_0 obtained by radiosonde can obtain better measurement results in the model of ESL inversion rainfall, we compare the rainfall inversed by ESL with the rainfall measured by Thies LPM. The result is shown in Fig. 5.

TABLE III
RAINFALL MEASUREMENT RESULTS OF THE ESL BASED ON h_0 FROM DIFFERENT SOURCES

h0	Rain intensity (mm/h)		Accumulated rain (mm)	
	RMSE	*CC*	*RMSE*	*CC*
ITU (4.67 km)	14.74	0.595	29.635	0.989
Radiosonde	9.052	0.872	17.504	0.995

TABLE IV
PERFORMANCE OF MEASURING TWO DIFFERENT KINDS OF RAINFALL BY THE ESL

Rainfall type	*RMSE*	*RE*	*CC*
Convective rainfall	7.871	16.01%	0.904
Stratiform rainfall	1.582	26.59%	0.804

In the retrieval of rainfall using the ESL, regardless of whether h_0 is based on the measured values obtained by radiosonde or the recommended values given by ITU-R, the inversion results of rainfall obtained by these ways are in good agreement with those of the Thies LPM. However, when h_0 is based on the recommended value given by the ITU-R recommendation, the inversion result of rain intensity for heavy rain is obviously low and the inversion result for light rain is obviously on the high side, which is mainly because in the actual rainfall process, the h_0 corresponding to heavy rain is lower and the h_0 corresponding to light rain is higher [17]. Therefore, the fixed average value of h_0 is higher than that of heavy rain and lower than that of light rain. In addition, when h_0 is based on the measured values obtained by radiosonde, the rain intensity inversion results of heavy rain and light rain are closer to those of the Thies LPM, and the deviation of the accumulated rainfall of the inversion results is smaller. The main reason may be that the h_0 obtained by radiosonde represents the actual height of the 0 °C-layer of the local atmosphere.

A combination of the root mean squared error (RMSE) and the correlation coefficient (CC) of the inversion results in Table III shows that the use of radiosonde in the rainfall inversion model of ESL will improve the accuracy of the inversion results, thereby improving the inversion performance of the calculation model. Therefore, in this article, when we use the ESL to retrieve rainfall events for the whole year of 2020, h_0 is obtained from the radiosonde data of the Nanjing reference climate station.

B. Statistical Analysis of the Rainfall Measurement Results

To test the accuracy and stability of the rainfall measurement results measured by the ESL, we use the ESL to retrieve continuous rainfall over a long period and compare the inversion results with the rainfall measurement results of the Thies LPM [35]. Fig. 6 shows the statistical results of the monthly accumulated rainfall in Nanjing measured by the ESL. From the statistical results of the ESL to the annual monthly accumulated rainfall, the measured value is close to that of the Thies LPM. From the statistical results, the overall CC between the monthly accumulated rainfall measured by the ESL and the monthly accumulated rainfall measured by Thies LPM is 0.985, and the

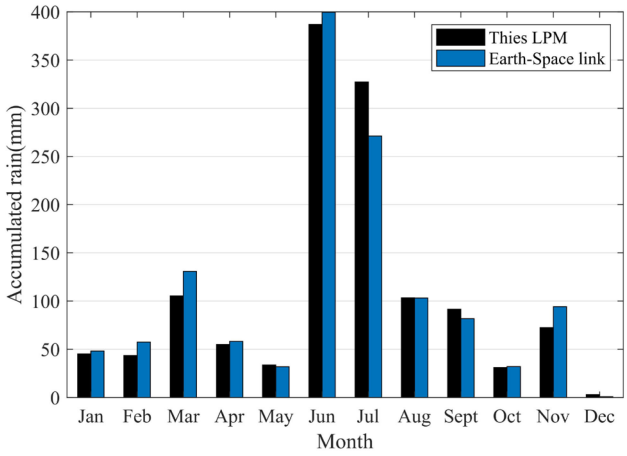

Fig. 6. Comparison between the statistical results of the monthly accumulated rainfall in Nanjing in 2020 measured by the ESL (blue bar) and the values measured by the Thies LPM (black bar).

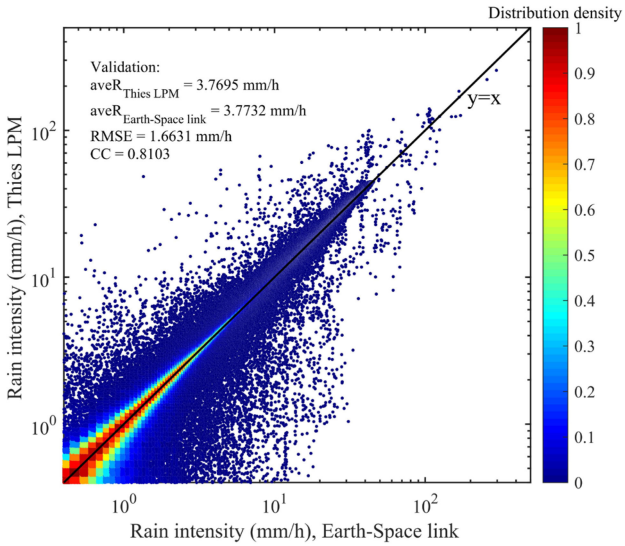

Fig. 7. Comparison of the rain intensity per minute throughout the whole year in Nanjing in 2020 measured by the ESL and measured by the Thies LPM.

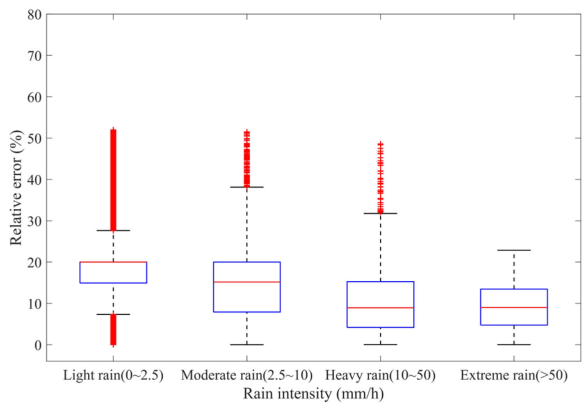

Fig. 8. Relative errors of light rain, moderate rain, heavy rain, and extreme rain as measured by the ESL. The red dots are outliers beyond the minimum and maximum of relative errors. The medians of the four boxes from left to right are 20%, 15.17%, 8.93%, and 8.99%, respectively.

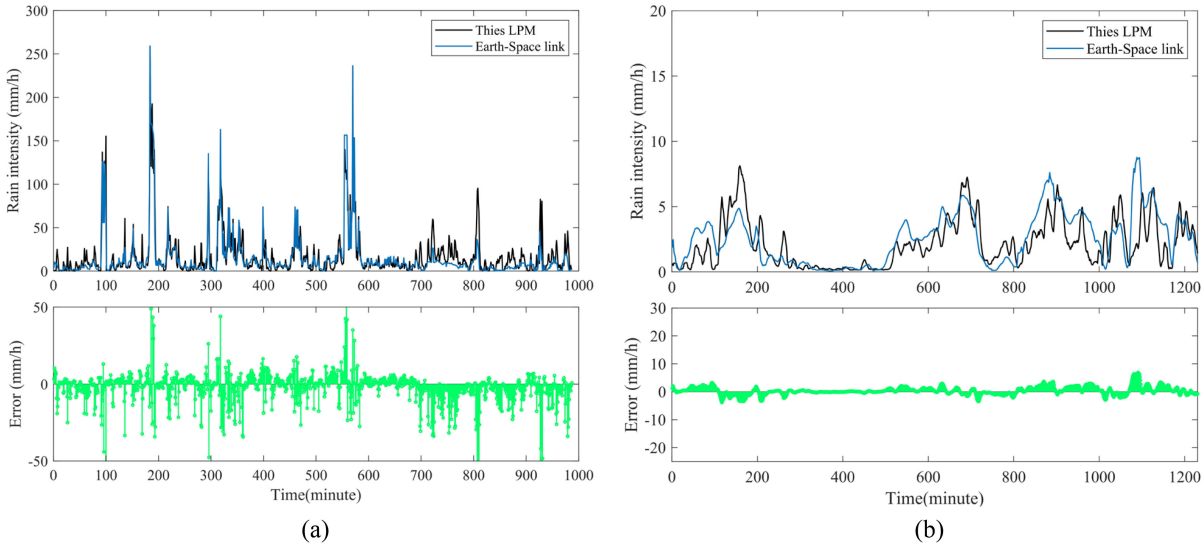

Fig. 9. Performance of measuring convective rainfall and stratiform rainfall by the ESL (blue line) during rainfall events from June to July in 2020. (a) Convective rainfall and (b) stratiform rainfall.

average RMSE is 19.841 mm. The large RMSE can be attributed to the obvious error that occurs during July, in which the ESL underestimates the rainfall significantly, compared with the Thies LPM. Noted that the high CC of the measurement results still means that the ESL can reflect the monthly accumulated rainfall of rainfall events in the process of continuous measurement over a year-long period.

Fig. 7 shows a comparison between the rain intensity inversed by the ESL and measured by the Thies LPM in 2020 (time resolution is 1 min). Since the actual rain intensity is mostly below 50 mm/h, here we use logarithmic coordinates to better observe the rain intensity close to the distribution of the coordinate axis. Although there is a certain number of the results of rain intensity inversed by the ESL with a large deviation, most of the results are close to the Thies LPM. The RMSE between the rain intensity from the ESL and from the Thies LPM is approximately 1.663 mm/h, and the CC is approximately 0.810. These findings indicate that the ESL has a better performance for the measurement of rain intensity.

On the basis of the above results, we divide rainfall events into light rain (0–2.5 mm/h), moderate rain (2.5–10 mm/h), heavy rain (10–50 mm/h), and extreme rain (>50 mm/h) according to the size of the rain intensity. The relative errors in different rain intensity categories are shown in Fig. 8. Noted that the relative errors of light rain, moderate rain, and heavy rain all appear as outliers in the measurement results, especially for light rain. The possible reason is that there is a higher relative error in light rain, which dominant the local rainfall throughout the year, as shown in Fig. 7. According to the distribution of the relative errors in Fig. 8, it can be found that the outliers of relative errors for the measurement results of different rainfall intensities decrease successively from light rain to extreme rain, and the medians of the four boxes from left to right are 20%, 15.17%, 8.93%, and 8.99%. The error of the inversion result of the ESL to the light rain is obviously large. The reason is that the attenuation of ESL caused by light rain is relatively weak, so it is difficult to distinguish the rainfall attenuation caused by light rain accurately from the noise caused by other factors. On the whole, the accuracy of rainfall inversion by the ESL increases with the increasing of rain intensity.

C. Measurement Performance of Different Rainfall Types

According to the development process and corresponding cloud system, natural rainfall is mainly divided into convective rainfall and stratiform rainfall [36], [37]. Significant differences were observed in the rain intensity and cumulative rainfall between the two types of rainfall. Therefore, convective rainfall and stratiform rainfall can be distinguished according to the stability of rain intensity over a time series [38]

$$\begin{cases} \text{Convective: } \sigma > 1.5 \text{ mm/h}, \& R_{t-5} \sim R_{t+5} > 5 \text{ mm/h} \\ \text{Stratiform: } \sigma \le 1.5 \text{ mm/h}, \& R_{t-5} \sim R_{t+5} > 0.5 \text{ mm/h} \end{cases} \tag{19}$$

where σ represents the standard deviation and R_{t-5} and R_{t+5} represent the rain intensity in the first 5 min and the last 5 min, respectively. According to this classification of rainfall, if the rain intensity from the first 5 min to the next 5 min at a certain time is more than 5 mm/h and the standard deviation of the rain intensity in this time period is more than 1.5 mm/h, then the rainfall at this time is convective rainfall. Correspondingly, if the rain intensity from the first 5 min to the next 5 min at a certain time is more than 1.5 mm/h and the standard deviation of the rain intensity during this time period is not more than 1.5 mm/h, then the rainfall at this time is stratiform rainfall [39].

To study the performance of ESL on retrieving the rainfall of different cloud systems, the rain intensity measured by the ESL and the Thies LPM are divided into convective rainfall and stratiform rainfall based on the above rainfall classification method. In this process, to ensure the continuity of rainfall events, we think that only rainfall events with a duration of more than 15 min can be analyzed. Fig. 9(a) and (b) describe the measurements result for convective rainfall and stratiform rainfall by ESLs

and the Thies LPM, respectively. With the measured value of the Thies LPM as a reference, the average RMSE of convective rainfall measured by the ESL is 7.871 mm/h and the CC is 0.904. Moreover, the average RMSE and CC of stratiform rainfall measured by the ESL are 1.582 mm/h and 0.804, respectively. In comparison, the convective rainfall and stratiform rainfall measured by the ESL are in good agreement with the measured values of the Thies LPM, although the correlation of convective rainfall is better than that of stratiform rainfall. In addition, from the RMSE of measuring different types of rainfall, the average RMSE of convective rainfall measured by the ESL is much larger than that of stratiform rainfall. This finding is mainly associated with the generally greater intensity of convective rainfall than stratiform rainfall, which prevents comparisons of the measured effect using the average RMSE alone. In addition to the average RMSE, we find that the average relative errors (RE) of convective rainfall and stratiform rainfall measured by the ESL are 16.01% and 26.59%, respectively. Combined with the average RMSE, RE, and CC of the measured results in Table IV, the performance of using the ESL to measure convective rainfall is better than that of stratiform rainfall. This finding also confirms that in the current research on ESL, there are many influencing factors that lead to instability in the measurement of stratiform rainfall with light rain intensity.

IV. Conclusion

As a new method, ESLs have shown considerable potential to measure rainfall for the large-scale monitoring of rainfall in the global atmosphere. In particular, the performance of ESL in practical applications will directly determine whether this new rainfall measurement technology can be widely used as an actual application in the future. In this article, to verify the practical applications of ESL for surface rainfall measurement, we set up an ESL device in Nanjing to monitor rainfall over a long period. First, we use the atmospheric 0 °C-layer height obtained from the radiosonde data of the Nanjing reference climate station to optimize the rainfall inversion model in the selection of 0 °C-layer of the ESL to measure rainfall and improve the accuracy of rainfall measurements. Second, we count the results of continuous long-term rainfall measurements of ESL and compare them with rain measurement data from the Thies LPM to study the measurement performance of ESL in continuous long-term measurements. Furthermore, we classify the results and study the performance of ESL in measuring different kinds of rainfall. From the study presented in this article, the main conclusions are as follows.

1) The actual height of the atmospheric 0 °C-layer is not a fixed value throughout a year but has obvious seasonal variation characteristics. If the atmospheric 0 °C-layer height data obtained from radiosonde data are applied to the study of ESL to retrieve rainfall, it will significantly improve the accuracy of the calculation model of ESL for measuring rainfall. This finding suggests that we can consider fusing multisource atmospheric data to optimize the calculation model in the selection of 0 °C-layer of ESL to measure rainfall in the future.
2) The ESL can be used to continuously monitor the actual rainfall and more accurately measure the monthly cumulative rainfall throughout the year. In addition, the performance of measuring rainfall by the ESL improves with increasing rain intensity, and the influencing factors of rainfall measured by the ESL have a greater impact on light rain.
3) The measurements of convective rainfall and stratiform rainfall by the ESL are in good agreement with the real rainfall values. However, the performance of measuring convective rainfall is better than that of stratiform rainfall.

This article only uses the data for the whole year of 2020 to verify the performance of continuous long-time rainfall retrieval by ESL in Nanjing. When using ESL to retrieve rainfall in different areas, the differences of position and elevation of the antenna, 0 °C-layer height h_0, and DSD of the local atmosphere should be taken into account. Considering that the rainfall measured by the ESL represents the average rainfall of the slant path, the rain intensity will differ from traditionally measured surface rainfall. However, with the implementation of communication satellite constellation, the ESLs have great potential to monitor rainfall of large-scale region and supplement traditional rainfall methods based on the overall performance. In the next step, we will continue to further study the performance of nonrainy factors on radio wave propagation in the complex atmosphere and validate the performance of this approach in different areas.

Acknowledgment

The authors thank the editor and anonymous reviewers for providing helpful advice. The data used in this study can be obtained from the corresponding author of this article.

References

[1] K. Goutam, K. M. Ashok, W. Yoshihide, and E. M. Michael, "Climate change will affect global water availability through compounding changes in seasonal precipitation and evaporation," *Nature Commun.*, vol. 11, Jun. 2020.
[2] G. L. Gragnani, M. Colli, E. Tavanti, and D. D. Caviglia, "Advanced real-time monitoring of rainfall using commercial satellite broadcasting service: A case study," *Sensors*, vol. 21, Jan. 2021, Art. no. 691.
[3] M. F. McCabe *et al.*, "The future of Earth observation in hydrology," *Hydrol. Earth Syst. Sci.*, vol. 21, May 2017.
[4] X. C. Liu, T. C. Gao, and L. Liu, "A comparison of rainfall measurements from multiple instruments," *Atmos. Meas. Tech.*, vol. 6, Jul. 2013.
[5] Z. Qingwei *et al.*, "Microphysical characteristics of precipitation during pre-monsoon, monsoon, and post-monsoon periods over the South China Sea," *Adv. Atmos. Sci.*, vol. 36, Oct. 2019.
[6] K. Song, X. Liu, and T. Gao, "Potential application of using smartphone sensor for estimating air temperature: Experimental study," *IEEE Internet Things J.*, to be published, doi: 10.1109/JIOT.2021.3063488.
[7] M. Hagit, Z. Artem, and A. Pinhas, "Environmental monitoring by wireless communication networks," *Science*, vol. 312, May 2006.
[8] H. Mostafa, S. I. S. Hassan, J. S. Mandeep, M. F. Ain, and H. A. Khedher, "Study of the effect of simulated rain on the offset parabolic antenna at Ku-band with different elevation angles," *Int. J. Antennas Propag.*, vol. 2007, pp. 1–5, 2007.
[9] O. Goldshtein, H. Messer, and A. Zinevich, "Rain rate estimation using measurements from commercial telecommunications links," *IEEE Trans. Signal Process.*, vol. 57, no. 4, pp. 1616–1625, Apr. 2009.
[10] A. Overeem, H. Leijnse, and R. Uijlenhoet, "Measuring urban rainfall using microwave links from commercial cellular communication networks," *Water Resour. Res.*, vol. 47, Dec. 2011.

[11] K. Song, X. Liu, and T. Gao, "Real-time rainfall estimation using microwave links: A case study in East China during the plum rain season in 2020," *Sensors*, vol. 21, Jan. 2021, Art. no. 858.
[12] M. Colli *et al.*, "A field assessment of a rain estimation system based on satellite-to-earth microwave links," *IEEE Trans. Geosci. Remote Sens.*, vol. 57, no. 5, pp. 2864–2875, May 2019.
[13] L. Barthès and C. Mallet, "Rainfall measurement from the opportunistic use of an earth–space link in the Ku band," *Atmos. Meas. Tech.*, vol. 6, pp. 2181–2193, Aug. 2013.
[14] E. Adirosi *et al.*, "Exploiting satellite Ka and Ku links for the real-time estimation of rain intensity," 2017, pp. 1–4.
[15] M. Colli *et al.*, "Rainfall fields monitoring based on satellite microwave down-links and traditional techniques in the city of Genoa," *IEEE Trans. Geosci. Remote Sens.*, vol. 58, no. 9, pp. 6266–6280, Sep. 2020.
[16] C. H. Arslan, K. Aydin, J. Urbina, and L. P. Dyrud, "Rainfall measurements using satellite downlink attenuation," in *Proc. IEEE Int. Symp. Geosci. Remote Sens. IGARSS*, Jul. 2014, pp. 4111–4114.
[17] C. H. Arslan, K. Aydin, J. V. Urbina, and L. Dyrud, "Satellite-link attenuation measurement technique for estimating rainfall accumulation," *IEEE Trans. Geosci. Remote Sens.*, vol. 56, no. 2, pp. 681–693, Feb. 2018.
[18] D. D. Huang, L. Xu, X. Feng, and W. Wang, "A hypothesis of 3D rainfall tomography using satellite signals," *J. Commun. Inf. Netw.*, vol. 1, Jun. 2016.
[19] L. Xu, X. Shen, D. D. Huang, X. Feng, and W. Wang, "Tomographic reconstruction of rainfall fields using satellite communication links," in *23rd Asia-Pacific Conf. Commun.*, 2017, pp. 1–5.
[20] L. Csurgai-Horváth, "Small scale rain field sensing and tomographic reconstruction with passive geostationary satellite receivers," *Remote Sens.*, vol. 12, Dec. 2020, Art. no. 4161.
[21] G. Bacci *et al.*, "The nefocast project: A nowcasting weather platform based on dual-frequency interactive satellite terminals," *XXXIInd General Assembly Scienti. Sympos. Int. Union Radio Sci.*, 2017, pp. 1–4, doi: 10.23919/URSIGASS.2017.8105126.
[22] F. Giannetti, M. Moretti, R. Reggiannini, and A. Vaccaro, "The NEFOCAST system for detection and estimation of rainfall fields by the opportunistic use of broadcast satellite signals," *IEEE Aerosp. Electron. Syst. Mag.*, vol. 34, no. 36, pp. 16–27, 2019.
[23] M. Xian, X. Liu, and T. Gao, "An improvement to precipitation inversion model using oblique earth-space link based on the melting layer attenuation," *IEEE Trans. Geosci. Remote Sens.*, vol. 59, no. 8, pp. 1–15, Aug. 2020.
[24] M. Xian, X. Liu, K. Song, and T. Gao, "Reconstruction and nowcasting of rainfall field by oblique earth-space links network: Preliminary results from numerical simulation," *Remote Sens.*, vol. 12, Nov. 2020, Art. no. 3598.
[25] L. Zhang *et al.*, "Intercomparison of solid precipitation derived from the weighting rain gauge and optical instruments in the interior Qinghai-Tibetan plateau," *Adv. Meteorol.*, vol. 2015, pp. 1–11, 2015.
[26] M. Angulo-Martínez, S. Beguería, B. Latorre, and M. Fernández-Raga, "Comparison of precipitation measurements by OTT Parsivel and Thies LPM optical disdrometers," *Hydrol. Earth Syst. Sci.*, vol. 22, pp. 2811–2837, May 2018.
[27] F. Giannetti *et al.*, "Real-time rain rate evaluation via satellite downlink signal attenuation measurement," *Sensors*, vol. 17, Aug. 2017, Art. no. 1864.
[28] M. Xian, X. Liu, M. Yin, K. Song, S. Zhao, and T. Gao, "Rainfall monitoring based on machine learning by earth-space link in the Ku band," *IEEE J. Sel. Topics Appl. Earth Observ. Remote Sens.*, vol. 13, pp. 3656–3668, Jun. 2020.
[29] R. Crane, "Prediction of attenuation by rain," *IEEE Trans. Commun.*, vol. 28, pp. 1717–1733, 2003.
[30] W. L. Stutzman and W. K. Dishman, "A simple model for the estimation of rain-induced attenuation along earth-space paths at millimeter wavelengths," *Radio Sci.*, vol. 17, pp. 1465–1476, 1982.
[31] M. J. Leitao and P. A. Watson, "Method for prediction of attenuation on earth-space links based on radar measurements of the physical structure of rainfall," in *Proc. IEE Proc. F - Commun., Radar Signal Process.*, vol. 133, 2008, pp. 429–440.
[32] ITU. *Recommendation ITU-R P.838-3 Specific Attenuation Model for Rain for Use in Prediction Methods*, 2005.
[33] ITU. *Recommendation ITU-R P .839 Rain Height Model for Prediction Methods*, 2013.
[34] X. Shen, D. D. Huang, W. Wang, A. F. Prein, and R. Togneri, "Retrieval of cloud liquid water using microwave signals from LEO satellites: A feasibility study through simulations," *Atmosphere*, vol. 11, May 2020, Art. no. 460.
[35] X. Liu, B. He, S. Zhao, S. Hu, and L. Liu, "Comparative measurement of rainfall with a precipitation micro-physical characteristics sensor, a 2D video disdrometer, an OTT PARSIVEL disdrometer, and a rain gauge," *Atmospheric Res.*, vol. 229, pp. 100–114, 2019.
[36] V. N. Bringi, V. Chandrasekar, J. Hubbert, E. Gorgucci, W. L. Randeu, and M. Schoenhuber, "Raindrop size distribution in different climatic regimes from disdrometer and dual-polarized radar analysis," *J. Atmos. Sci.*, vol. 60, pp. 354–365, 2003.
[37] K. Pu, X. Liu, H. He, Y. Sun, S. Hu, and Y. Wu, "Microphysical characteristics of winter precipitation in Eastern China from 2014 to 2019," *Water*, vol. 12, Mar. 2020, Art. no. 920.
[38] C. Baojun, Y. Jun, and P. U. Jiangping, "Statistical characteristics of raindrop size distribution in the Meiyu season observed in Eastern China," *J. Meteorol. Soc. Jpn. Ser. II*, vol. 91, Oct. 2013.
[39] K. Pu, X. Liu, S. Hu, and T. Gao, "Hydrometeor identification using multiple-frequency microwave links: A numerical simulation," *Remote Sens.*, vol. 12, Jul. 2020, Art. no. 2158.

Yingcheng Zhao received the B.S. degree in atmospheric measurement techniques from the National University of Defense Technology, Nanjing, China, in 2020, where he is currently working toward the M.S. degree in atmosphere science.

His research interests include atmospheric physics, atmospheric measurement, and remote sensing techniques and instruments.

Xichuan Liu received the M.S. and Ph.D. degrees in atmospheric measurement techniques from the PLA University of Science and Technology, Nanjing, China, in 2010 and 2014, respectively.

He is currently an Associate Professor with the College of Meteorology and Oceanography, National University of Defense Technology, Nanjing, China. His research interests include atmospheric physics, atmospheric measurement, and remote sensing techniques and instruments.

Minghao Xian received the M.S. degree in atmospheric sciences from the National University of Defense Technology, Nanjing, China, in 2020. His research interests include atmospheric physics, atmospheric measurement, and remote sensing techniques and instruments.

Taichang Gao received the B.S. degree in dynamic meteorology from the Air Force College of Meteorology, Nanjing, China, in 1982.

He is currently a Professor with the College of Meteorology and Oceanography, National University of Defense Technology, Nanjing, China. His research interests include atmospheric measurement and remote sensing techniques and instruments.